ACS OMEGA

http://pubs.acs.org/journal/acsodf

Article

Synthesis of Mesoporous Carbon Adsorbents Using Biowaste Crude Glycerol as a Carbon Source via a Hard Template Method for Efficient CO_2 Capture

Prabhu Azhagapillai,* K. Suresh Kumar Reddy, Gerardo D. J. Guerrero Pena, Rukayat S. Bojesomo, Abhijeet Raj,* Dalaver H. Anjum, Mirella Elkadi,* Georgios N. Karanikolos, and Mohamed I. Ali

Cite This: *ACS Omega* 2023, 8, 21664−21676

Read Online

ACCESS | Metrics & More | Article Recommendations

ABSTRACT: Biowaste utilization as a carbon source and its transformation into porous carbons have been of great interest to promote environmental remediation owing to biowaste's cost-effectiveness and useful physicochemical properties. In this work, crude glycerol (CG) residue from waste cooking oil transesterification was employed to fabricate mesoporous crude glycerol-based porous carbons (*m*CGPCs) using mesoporous silica (KIT-6) as a template. The obtained *m*CGPCs were characterized and compared to commercial activated carbon (AC) and CMK-8, a carbon material prepared using sucrose. The study aimed to evaluate the potential of *m*CGPC as a CO_2 adsorbent and demonstrated its superior adsorption capacity compared to AC and comparable to CMK-8. The X-ray diffraction (XRD) and Raman results clearly depicted the structure of carbon nature with (002) and (100) planes and defect (D) and graphitic (G) bands, respectively. The specific surface area, pore volume, and pore diameter values confirmed the mesoporosity of *m*CGPC materials. The transmission electron microscopy (TEM) images also clearly revealed the porous nature with the ordered mesopore structure. The *m*CGPCs, CMK-8, and AC materials were used as CO_2 adsorbents under optimized conditions. The *m*CGPC adsorption capacity (1.045 mmol/g) is superior to that of AC (0.689 mmol/g) and still comparable to that of CMK-8 (1.8 mmol/g). The thermodynamic analyses of the adsorption phenomena are also carried out. This work demonstrates the successful synthesis of a mesoporous carbon material using a biowaste (CG) and its application as a CO_2 adsorbent.

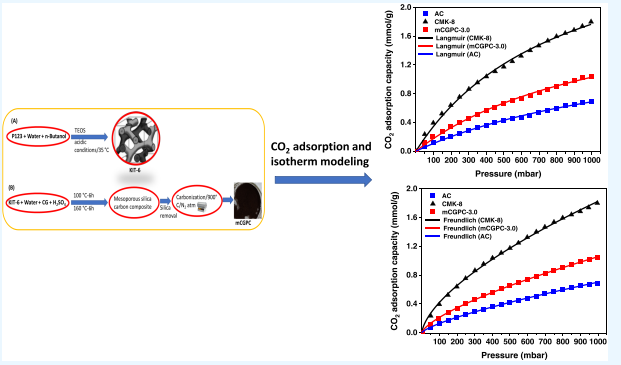

1. INTRODUCTION

CO_2 emission from the combustion of fossil fuels is known to contribute to global warming and climatic change.[1−3] In the past two decades, near-real-time data indicate that global CO_2 emissions have increased by 43.5 ppm (equivalent to a 12% rise). Hence, significant research is focused on exploring alternative energy sources such as solar, biomass, and other renewable energies. One of the existing solutions to combating rising CO_2 levels is capturing CO_2 from its sources or from ambient air with modern adsorption technologies.[4] In this context, numerous robust adsorbent materials such as zeolites, activated carbons (ACs), metal−organic frameworks, and porous polymers have been fabricated for their large-scale applications for carbon capture and storage.[5−7] Along with the existing carbon capture technologies, the enhancement of CO_2 adsorption capacity has become a present-day research interest. This is on the grounds of economic as well as productivity improvements. Basic properties of adsorbent materials include surface activation, high thermal stability, high abrasion resistance, and average pore diameters with a high exposed surface area that results in high adsorption capacity.[8,9] Nonetheless, the fabrication of solid adsorbents with high porosity, tuned functionality, surface structural features, and stability is a challenge and much effort has been devoted to exploring the effective adsorbents to improve CO_2 capture through adsorption.[10−12] In general, CO_2 possesses a strong tetrapolar character and weak acidity, and the activated carbons with basic compounds achieve good adsorption. Several methods to fabricate porous carbon materials with surface activation are considered vital to enhance the CO_2 adsorption capacity.[13−15] Ordered spherical mesoporous carbons with large pores and volumes were synthesized using

Received: February 17, 2023
Accepted: May 12, 2023
Published: June 5, 2023

cellular foam as a template and lignin as the carbon source. They show high Brunauer–Emmett–Teller (BET) surface areas and CO_2 adsorption capacity (2.95 mmol-CO_2), which is higher than that of other mesoporous carbons. These were synthesized via a hard-templating method, and preparation conditions played a role in achieving the desired properties.[16] Wang[17] and colleagues have reported that peanut shells can be used to produce low-cost porous carbon materials through activation with either KOH or K_2CO_3. According to their study, the K_2CO_3-activated peanut shells in particular exhibited excellent performance in both CO_2 adsorption and regeneration. Hack[18] and his team have written a review that summarizes the capacity of amine-functionalized materials to adsorb CO_2. The review discusses a range of porous solid materials, including zeolites and metal–organic frameworks, which have been reported to exhibit this capability.

In this regard, ordered mesoporous carbons (OMCs) have attracted great interest in CO_2 adsorption.[19,20] OMCs possess a wide range of ordered pore channels and are especially useful for the separation of large molecules by providing extensively fast mass transfer that is highly advantageous in heterogeneous catalysis.[21,22] The current two methods used for OMCs' fabrication are the hard-templating strategy using organic polymerization with the inverse replication of the template [e.g., MCM-48, KIT-6, SBA-*n* (n = 1, 7, 15)] and the soft-templating route via supramolecular self-assembly between amphiphilic nonionic copolymers and phenolic resins. There remains scope for making advancements in efficient surface and textural properties.[23−31] In this direction, several mesoporous carbon materials with diverse structures and a wide range of porosity and physicochemical properties have been fabricated.[20,32] The structure and pore sizes of the produced carbon material depend on the carbon precursors used, the nature of the silica template, the reaction time, temperature, and the carbonization process. The structure still lacks uniformity due to mere structural collapse during carbonization. Hence, it is challenging to produce mesoporous carbons since the synthesis conditions, such as carbon-to-silica ratio and the choice of carbon precursors, need to be varied and optimized.[20,33−35]

Various carbon sources are of interest to synthesize OMCs, and approaches from bio-based carbon compounds as precursors are crucial for eco-friendly management. More specifically, when refined and recycled bio-wastes, specifically derived from food scraps, have the potential to be a sustainable alternative. Considering disposal regulations and the use of those food wastes as cheap starting materials, biorefineries have been of significant interest in the current value-based market.[36,37] There is an annual availability of more than 15 million tons of waste cooking oil (WCO).[38,39] Crude glycerol (CG) is the main byproduct generated during biodiesel production by transesterification of WCO, where 0.10 kg of CG is generated per kg of biodiesel produced.[40] The complications and high costs associated with biodiesel production encourage the development and utilization of CG produced as a byproduct. For instance, CG could be utilized as a feed source for carbon materials.

Like pure glycerol, CG could be employed as a pore-forming agent for mesoporous silica and as a carbon precursor for OMCs.[41,42] The derived materials could possess micropores and large mesopores due to some impurities present in CG, such as soap and fatty acid methyl ester. Further, the size and concentration of glycerol could affect the porosity and morphology of the formed OMC possessing semigraphitic pore walls. Moreover, the synthesis method and the nature of CG could offer distinct mesoporous carbons with high surface area and tailorable porosity. Such altered surface chemistry in porous carbon species could be achieved by utilizing CG under different experimental conditions. To date, the development of biowaste carbon sources for porous carbon production is still highly challenging because of several demanding criteria, such as a regulated pore structure, activating the surface carbon, and enhanced surface area, thereby affecting the adsorption capacity of CO_2.

Motivated by the increased attention to global CO_2 capture and finding effective biowaste-processed porous carbon adsorbents, the objectives of this work are to (i) use CG from WCO as a carbon source to synthesize porous carbon (CGPC) and compare it with conventional activated carbons and prominent CMK-8 materials, and (ii) study the potential application of CGPC as an adsorbent for CO_2. A protocol for designing porous carbons from impure biowaste precursors with altered surface properties, high porosity, and thermal stability is presented. The characterization of the textural properties and surface chemistry of *m*CGPC materials is used to explain the CO_2 adsorption performance, especially at low CO_2 partial pressures.

2. EXPERIMENTAL SECTION

2.1. Materials and Chemicals. Pluronic P123 (M_W = 5800), tetraethyl orthosilicate (TEOS), butanol (C_4H_9OH), hydrochloric acid (HCl), sulfuric acid (H_2SO_4), hydrofluoric acid (HF), and sucrose were received from Sigma Aldrich and were used as received. The commercial NORIT activated carbon (AC) was received from the Cabot Corporation, where it was synthesized using a peat-based carbon source (activated using steam) and contained particles of 2–4 mm diameter. Crude glycerol was obtained from waste cooking (canola) oil transesterified in our laboratory, and deionized water was used during the synthesis.

2.2. Synthesis of Mesoporous Silica, KIT-6. KIT-6 was synthesized using soft templating and hydrothermal procedures previously described.[43,44] Pluronic P123 (4 g) was dissolved in 150 mL of distilled water, and 7.9 g of concentrated HCl was added dropwise under constant stirring at room temperature. The solution mixture was continuously stirred for 3 h to complete the dissolution of the template. After 3 h, 4 mL of butanol was added to the solution while maintaining the same stirring condition for another 1 h. Thereafter, 8.4 g of TEOS was added dropwise and continuously stirred at 35 °C for 24 h. The vigorous stirring is essential to obtain the high porosity of the mesoporous silica. The white-colored solution was kept in a drying oven at 100 °C for 24 h. After cooling it to room temperature, the solution was filtered and washed with distilled water and ethanol. Then, the final product was dried in an oven at 100 °C for 12 h. Later, the white precipitate powder was finely ground and kept in a muffle furnace at 550 °C for a 6 h calcination process to remove the template.

2.3. Synthesis of Mesoporous Carbon, CMK-8. Mesoporous silica KIT-6 is required to prepare the mesoporous carbon (silica as a template source) with the ordered porous structure of CMK-8. Sucrose (0.75 g) was dissolved in distilled water (5 g) to form a clear solution (sucrose was employed as a carbon precursor). Then, the parent silica KIT-6 (0.5 g) was dispersed in the same solution.

https://doi.org/10.1021/acsomega.3c01083
ACS Omega 2023, 8, 21664−21676

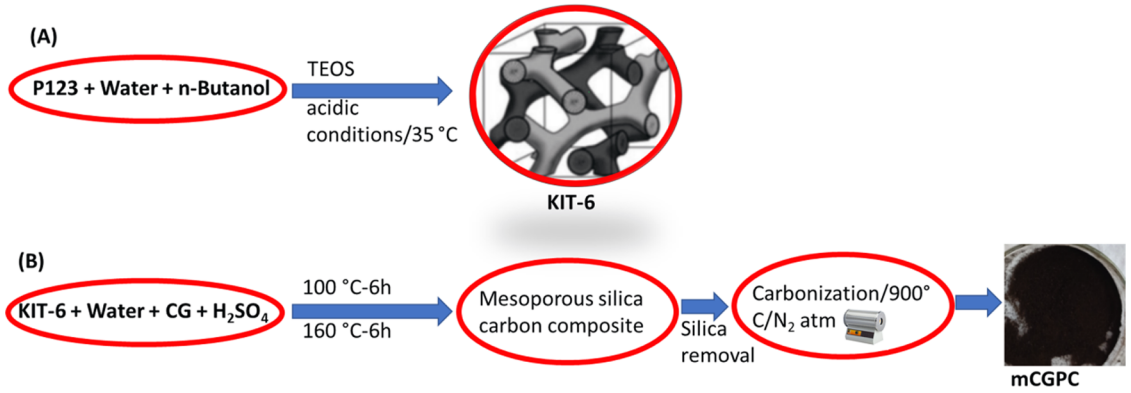

Figure 1. Schematic of the synthesis procedure of mesoporous silica and *m*CGPC.

Subsequently, 0.15 g of sulfuric acid was added dropwise to the clear solution and mixed into a paste form and then kept in an oven for a complete pore-filling process. The composite was treated at 100 °C for 6 h and then at 160 °C for another 6 h. A similar procedure was repeated with the same condition for the perfect impregnation of the carbon precursor. A brownish-colored solid material was produced. It was then crushed into a fine powder and then subjected to a carbonization process at 900 °C with a heating ramp of 10 °C/min for 6 h under nitrogen gas for complete carbonization of mesoporous carbon. After this process, the black-colored powder was mixed with a solution of 5% HF in water for 6 h stirring at room temperature to remove the silica template. Then, the solution mixture was washed with ethanol and dried at 100 °C for 12 h to obtain CMK-8.

2.4. Production of Crude Glycerol (CG). Crude bioglycerol was produced from waste canola oil. First, 20 g of canola oil was weighed and transferred into a two-neck round-bottom flask after being preheated at 240 °C for 2 h (the oil was subjected to a high temperature for a sufficient time to produce a waste cooking oil). To the preweighed oil, 50% of the methanol solution (12:1 methanol/oil molar ratio) and KOH (1.0 wt %) were added and stirred for 10 min at room temperature. The temperature was then raised to 50 ± 5 °C and left in a reflux setup for 60 min. The product (mixture of biodiesel and crude bioglycerol) was transferred into a separating funnel and left to stand until two distinct bilayers were observed. The bottom layer containing the crude bioglycerol was collected and employed for further analysis without any prior purification.

2.5. Synthesis of Crude Glycerol-Mesoporous Carbon (*m*CGPC). KIT-6 is used as the silica template to prepare the crude glycerol-based porous carbon (*m*CGPC). The mesoporous silica KIT-6 (0.5 g) was mixed with 5 g of distilled water in a Petri dish, and then, 0.5 mL of crude bioglycerol was slowly added and mixed properly to form a paste. Concentrated sulfuric acid (0.15 g) was added to the paste and then mixed vigorously until the formation of a homogeneous gel. The composite mixture was kept in the oven at 100 °C for 6 h. Then, the temperature was increased, and the mixture was kept at 160 °C for another 6 h. To obtain the *m*CGPC-*x* materials (x = 0.5, 1.0, and 3.0 mL), a comparable procedure was employed where varying amounts of crude bioglycerol were impregnated into the silica pores. The process of impregnating the carbon precursor and subsequent carbonization, as well as the removal of silica, in the second step, followed the same procedure outlined in Section 2.3. A higher amount of crude glycerol would lead to pore blockage due to its high kinetic diameter; therefore, 3 mL was optimum for *m*CGPC preparation. Figure 1 presents a simplified diagram of the procedure to prepare *m*CGPC.

2.6. CO_2 Adsorption Experiments. The CO_2 adsorption test of all of the adsorbents was conducted using a Micromeritics 3Flex Analyzer in the static volumetric mode. The CO_2 adsorption isotherms were collected at 25 and 45 °C at pressures of up to 1 bar in the pressure steps of 50 mbar. Similarly, N_2 adsorption isotherms were collected at 25 °C at pressures of up to 1 bar in the pressure steps of 50 mbar. A fresh sample of approximately 100 mg was used for each adsorption run. Prior to the analysis, the adsorbents were degassed at 200 °C with a ramp rate of 5 °C under a high vacuum for 6 h to remove any trapped volatile matter carried from their synthesis and water vapor adsorbed from ambient air. The CO_2 and N_2 adsorption findings were evaluated using the dry weight of each adsorbent. In addition, CO_2/N_2 selectivity was calculated at 1 bar, and the recyclability of adsorbents was tested using pressure swing adsorption (PSA) to check the reusability of the adsorbents and also determine the isosteric heat of adsorption.

2.7. Characterization Techniques. The X-ray diffraction (XRD) patterns in the 2θ ranges of 10−60° of the materials were recorded by a Bruker D2 Phaser. The scan range of 10−60° was used with a step size of 0.03° and a scan speed of 10 s/step.

Raman spectroscopy (WITec, Germany) was used to conduct the structural analysis of the synthesized and commercial carbons. The samples were placed on a glass plate, and each spectrum was collected with a resolution of 2 cm^{-1} in the 1090−2000 cm^{-1} range. The excitation wavelength was 532 nm with an energy setting of 1.2 mV, and the spectra were collected using backscattering geometry with an acquisition time of 50 s.

The surface morphology of samples was obtained by scanning electron microscopy (SEM, Quanta 3D operated at 30 kV). Before the SEM analysis, the samples were coated with a thin layer of gold.

The N_2 adsorption−desorption isotherms of the samples were measured at −196 °C on a Micromeritics 3-flex instrument. Samples were degassed for 10 h at 200 °C under a vacuum before being measured. The Brunauer−Emmett−Teller (BET) method was used to determine the specific surface areas of the samples. The Barrett−Joyner−Halenda approach was used to obtain the pore-size distributions from the adsorption branches of the isotherms. At a P/P_0 of 0.99,

https://doi.org/10.1021/acsomega.3c01083
ACS Omega 2023, 8, 21664−21676

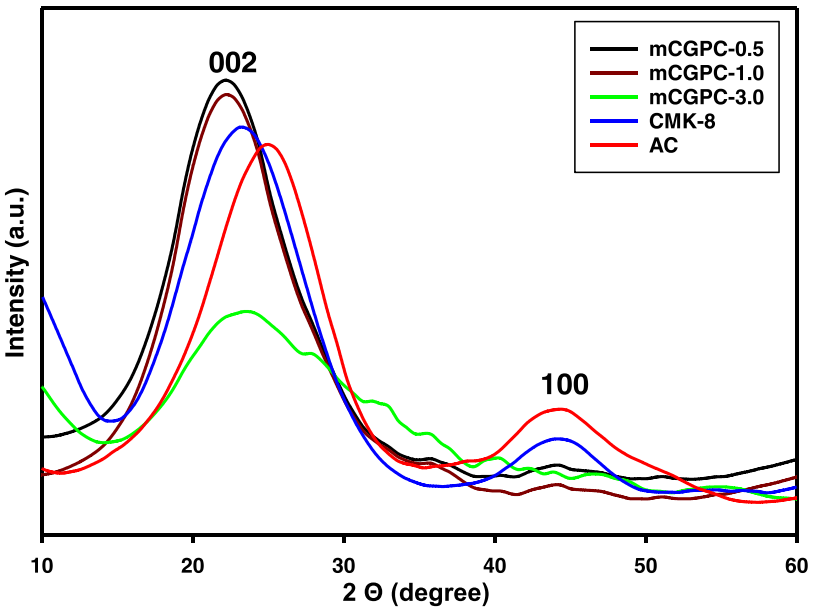

Figure 2. XRD patterns of *m*CGPC, CMK-8, and AC materials.

the total pore volume (V_t) was calculated from the N_2 adsorption branches.

A buoyancy experiment employing an Intelligent Gravimetric Analyzer (IGA), developed by Hiden, U.K., was used to determine the skeletal density of the adsorbents. The skeletal densities of CMK-8, AC, and *m*CGPC-3.0 were calculated by a buoyancy experiment that used helium flow up to 6 bar in stages of 1 bar as 1.254, 2.212, and 1.147 g/cm^3, respectively.

A high-resolution transmission electron microscope (HRTEM, TITAN) operating at 120 kV was used to characterize the nanostructures in the materials. The material was first ultrasonically dispersed in ethanol, and then, this suspension was dropped onto a porous carbon film-covered copper grid for HRTEM imaging.

The surface chemistry and bonding interactions were analyzed by an attenuated total reflective Fourier transform infrared (ATR-FTIR) spectrometer, and the synthesized materials were acquired using a Bruker Alpha-Platinum ATR in the range of 500−4000 cm^{-1} with a scan rate of 24 scans per minute and a nominal resolution of 2 cm^{-1}.

The thermal stability of the synthesized carbons was studied using a thermogravimetric analyzer (TGA Perkin Elmer STA 6000). The samples were heated in an air atmosphere from room temperature to 900 °C for complete burnt-out at the heating rate of 10 °C/min, and their mass loss profiles were recorded. The flow rate of air was fixed at 20 mL/min throughout the analysis.

3. RESULTS AND DISCUSSION

3.1. Adsorbent Characterization. *3.1.1. X-ray Diffraction (XRD) Patterns.* The wide-angle XRD patterns of the *m*CGPC, CMK-8, and AC samples are shown in Figure 2.

The primary peaks at 2θ = 23 and 43° corresponded to the (002) and (100) diffraction planes of the graphitic frameworks, respectively, and no further peaks were seen.[45] This result demonstrates that, after the pyrolysis at 900 °C in a nitrogen environment, all of the samples are entirely carbonized and the broadness of the peaks indicates that these materials are partially amorphous in nature. The (002) peak is assigned to the interlayer diffraction resulting from the stacks of parallel planes, and the intralayer (100) peak represents the clusters of graphene sheets. In comparison, the activated carbon and CMK-8 samples show a very broad peak indicating a high degree of graphitization. The *m*CGPC-(0.5−1.0) peaks show a higher graphitization degree than *m*CGPC-3.0, and it indicates the influence of the amount of crude glycerol on the formation of mesoporous carbon in a porous silica matrix. At low concentrations, a majority of CG enters the silica pores to lead to linked carbon structures in the pores; however, at high CG loading (3.0 mL), some glycerol may carbonize on the surface outside the silica pores to lead to its amorphous character (less graphitic character). Due to this reason, the carbon formation and the peaks are weaker than the other *m*CGPCs, which is also evidenced by Raman analysis and SEM morphology (shown later).

To study the variation in the structural properties of carbonaceous samples with increasing glycerol content, three parameters were derived using the XRD pattern: (a) polycyclic aromatic hydrocarbon (PAH) interlayer spacing (d_{002}) using Bragg's law, as shown by eq 1; (b) the nanocrystallite height (L_c) using the Scherrer formula (eq 2), which indicates the thickness of the PAH stacks; and (c) the nanocrystallite length (L_a) using the Scherrer formula (eq 3), which indicates the average length of PAHs.

$$d_{002} = \frac{\lambda}{2 \sin \theta_{002}} \tag{1}$$

$$L_c = \frac{0.9\lambda}{B_{002} \cos \theta_{002}} \tag{2}$$

$$L_a = \frac{1.84\lambda}{B_{002} \cos \theta_{002}} \tag{3}$$

In the above equations, λ represents the wavelength (for Cu Kα radiation, λ = 1.54 A), θ_{002} is the Bragg angles, and B_{002} is the full width at half-maximum (FWHM) for the (002) peak. To obtain Bragg's angle and FWHM, Gaussian curves were fitted through the (002) peak using Matlab software.

https://doi.org/10.1021/acsomega.3c01083
ACS Omega 2023, 8, 21664−21676

Table 1 provides the values of these structural parameters for the carbonaceous samples. The interplanar distances in all of

Table 1. Structural Parameters of *m*CGPC, CMK-8, and AC Samples Obtained from XRD Pattern Analysis

sample name	interplanar distance (d_{002}) (Å)	nanocrystallite height (L_c) (Å)	nanocrystallite length (L_a) (Å)
*m*CGPC-0.5	4.03	20.74	42.87
*m*CGPC-1.0	4.04	19.74	40.80
*m*CGPC-3.0	3.80	7.21	14.91
AC	3.61	12.17	25.16
CMK-8	3.69	9.41	19.45

the samples are greater than that of graphite (0.33 nm). The difference suggests that all of the samples have extended PAH layers due to the amorphous characteristics. When the glycerol content increases from 0.5 to 1.0 g during sample preparation, there is a very small change in nanostructural parameters. However, with an increase in the glycerol content to 3.0 g, the produced carbon possessed a lower interplanar distance, shorter PAH stacks, and smaller PAHs when compared to *m*CGPC-(0.5−1.0), indicating an increase in the amorphous nature.

3.1.2. Raman Spectra. Raman spectroscopy was used to learn more about the porous carbon structure and surface topology of all carbons, as illustrated in Figure 3.

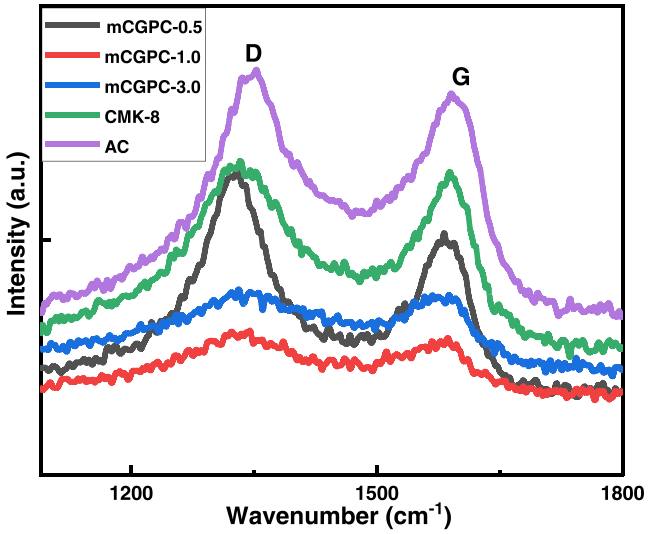

Figure 3. Raman spectra of *m*CGPC, CMK-8, and AC materials.

The Raman spectra of *m*CGPC, CMK-8, and AC reveal the degree of disorder in the materials. In general, carbon-based samples show peaks at roughly 1331−1348 and 1576−1593 cm^{-1} for the D and G bands, respectively. These two bands were observed for all of the samples (with some differences in peak positions, as shown in Table 1) due to the different nature of carbon samples and/or their starting materials. The D band, which appears around 1331 cm^{-1}, is most likely caused by lattice defects (sp^3 carbon) or other impurities[45,46] and is indicative of the amount of amorphous carbon in the material.

The G band was found near 1576 cm^{-1}, which is a result of the sp^2 hybridized carbon in-plane stretching vibration, and its amplitude indicates the amount of crystalline graphitic carbon. To assess the relative amounts of disordered and graphitic carbons in the materials, the ratios of the intensities of the G band and the D band (I_G/I_D) were found, whose values for the different materials are shown in Table 2. The intensity ratios

Table 2. G and D Bands and Their Intensity Ratios

sample	D band (cm^{-1})	G band (cm^{-1})	I_G/I_D
*m*CGPC-0.5	1331	1585	0.986
*m*CGPC-1.0	1333	1576	0.998
*m*CGPC-3.0	1335	1588	0.998
CMK-8	1333	1589	0.997
AC	1348	1593	0.994

are about 1 for all of the porous carbons, which indicates that the amount of crude glycerol (carbon precursor) used for *m*CGPC preparation did not significantly affect the carbon structure.

3.1.3. Scanning Electron Microscopy (SEM) Images. The morphologies of all of the carbon materials were characterized by scanning electron microscopy (SEM), and the images are shown in Figure 4. The activated carbon surface exhibits a smooth morphology with large particle size, accompanied by irregular cavities and a well-developed porous structure, which is consistent with findings reported in the literature.[47] In contrast to activated carbon, the pristine CMK-8 sample has a worm-like mesoporous structure, which comprises numerous micrometer-sized rod-like particles to result in high porosity. The *m*CGPC-0.5 images show an irregular surface morphology with rod-like and worm-like structures that are inherited from the mesoporous silica replica. The *m*CGPC-1.0 sample surface morphology shows irregular shapes of a smooth morphology together with rod- and worm-like structures with a blurry surface. The *m*CGPC-3.0 surface also had an irregular shape with a rod- and worm-like shape, indicating that an increase in the CG amount did not noticeably destroy the structure of the porous carbon. However, the surface roughness increases with an increase in CG loading.

3.1.4. Fourier Transform Infrared (FTIR) Spectra. The ATR/FTIR spectra were used to determine the carbon and oxygen functional groups on *m*CGPC, CMK-8, and AC materials (Figure 5).

All of the carbon materials exhibited characteristic bands around 3440−3550 cm^{-1} for −OH stretching or adsorbed water molecules. The band observed at around 2380 cm^{-1} is assigned to the C≡C stretching vibration of the aromatic carbon network.[48] The band at around 1652 cm^{-1} is attributed to the bending vibration of carbonyl groups, C═O. The band at 1280 cm^{-1} is assigned to C−O bonds of the carboxyl group. The signals at around 1920−2315 cm^{-1} are the characteristics of ATR measurements.[49] The ATR/FTIR results indicate the presence of carboxylic, carbonyl, and hydroxyl groups on *m*CGPC and CMK-8 samples, expectedly, due to the presence of oxygen functionalities in the starting material for these mesoporous carbon syntheses, while the AC sample had relatively less pronounced peaks for these oxygenated groups.[50]

3.1.5. Thermogravimetric Analysis (TGA). Figure 6 shows the TGA profiles of the CMK-8, *m*CGPCs, and AC samples in an air environment while varying the temperature. The initial weight loss below 200 °C is due to the physisorbed water molecules and loosely bound volatile matter on the samples. The second weight loss occurs in the range of 200−400 °C due to the presence of reactive oxygenated functional groups that

https://doi.org/10.1021/acsomega.3c01083
ACS Omega 2023, 8, 21664−21676

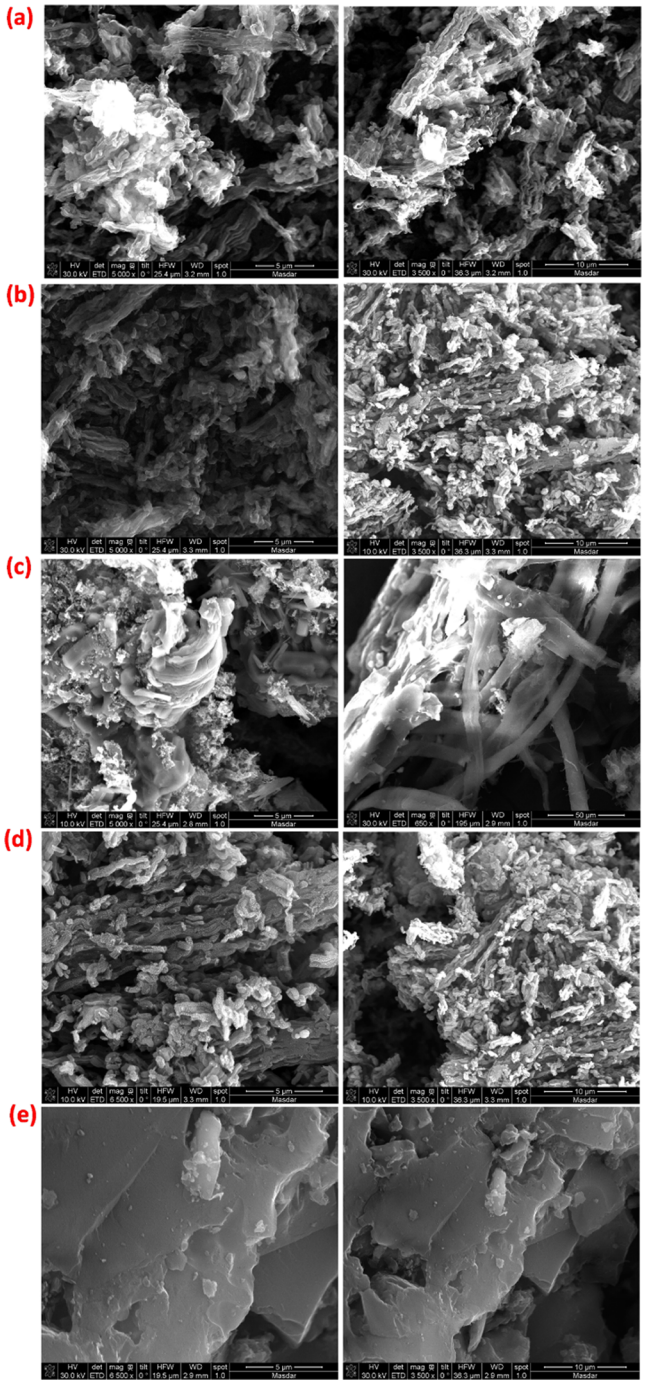

Figure 4. SEM images of *m*CGPC, CMK-8, and AC at different magnifications: (a) *m*CGPC-0.5; (b) *m*CGPC-1.0; (c) *m*CGPC-3.0; (d) CMK-8; and (e) AC.

can support carbon oxidation at relatively low temperatures. However, this is more apparent for the AC sample possibly due to the presence of oxygenated groups on the surface that can be easily desorbed. The *m*CGPC-0.5 and *m*CGPC-1.0 samples had similar weight loss profiles due to the similar nature of the porous network. However, *m*CGPC-3.0 suffered a relatively higher weight loss at low temperatures, which could be due to its less graphitic character (as indicated by the XRD pattern) and the presence of more loosely bound volatiles than the other *m*CGPC samples. After 200 °C, the weight loss was slow with increasing temperature, indicating the stability of the carbon framework at such temperatures. The sudden weight loss occurred after 550 °C due to the combustion of carbon. At around 624 °C, the *m*CGPC samples were completely burnt. There was no leftover mass after the complete combustion, which indicates that the silica framework was completely removed from the materials during their preparation. The TGA profiles show complete combustion at a maximum temperature of 900 °C for all of the materials. These profiles also indicate the thermal stability of the materials at moderately high temperatures in the air environment in the following order: CMK-8 > *m*CGPC-1.0 > *m*CGPC-0.5 > AC > *m*CGPC-3.0.

3.1.6. Transmission Electron Microscopy (TEM) Images. The TEM images of all of the synthesized materials are shown in Figure 7. Figure 7a shows a long-ranged ordered three-dimensional cubic (*Ia*3*d* symmetry) mesostructure in CMK-8 with tube-like channels and an interpenetrating bicontinuous network of channels.[51] Figure 7b,c shows a similar structure for the *m*CGPC samples, but the structure is slightly less-ordered in the bicontinuous porous network. Especially, the CGPC-3.0 sample shows a very less ordered structure due to the low interconnectivity between the pore channels[52] (which was also apparent from XRD and RAMAN results and the nitrogen adsorption results shown later).

3.1.7. N_2 Adsorption Isotherms. Figure 8a shows the nitrogen adsorption isotherms of *m*CGPCs, AC, and CMK-8 materials, and Figure 8b,c shows their microporous and mesoporous pore volume and pore diameter distribution. The nitrogen sorption experiments were conducted at −196 °C to study the role of textural characteristics and to determine the effects of activation conditions on the micro- and meso-structures of carbons. The results are summarized in Table 3. According to the IUPAC classification, *m*CGPC and CMK-8 isotherms are type IV and show H1 hysteresis with a prominent capillary condensation in the mesopores, confirming the presence of well-ordered mesopores.[53] The AC isotherm resembles type I.[54] The isotherm can be classified as reversible type I because of the concave profile, the high nitrogen amount adsorbed at low P/P_0 values, and the plateau at the high P/P_0 values for both adsorption and desorption branches. This type of isotherm is typical of materials with molecular-scale micropores, where micropore filling is the dominant mechanism at low P/P_0. All of the adsorbents exhibit a high specific surface area in the range from 388 to 1085 m^2/g and the total pore volume ranging from 0.262 to 1.027 cm^3/g. For *m*CGPCs, with increasing crude glycerol content (0.5−3.0) during sample preparation, the surface area increased along with the total pore volume and the micropore volume. This indicates an increase in the porous nature of the material with increasing glycerol concentration. The CMK-8 material possesses a very high surface area as compared to the others possibly due to the purity of the carbon precursor used (pure sucrose as opposed to crude glycerol for *m*CGPC) and the cyclic structure of sucrose that could help in the formation of aromatic structures of high order.

3.2. CO_2 and N_2 Adsorption. The carbon dioxide (CO_2) adsorption experiments were carried out at 25 and 45 °C up to 1 bar pressure, and the isotherms are shown in Figure 9a,b. The CO_2 adsorption capacity in mmol/g for all of the adsorbents is listed in Table 3. While CMK-8 had the highest capacity (1.8 mmol/g) and AC had the lowest one (0.7 mmol/g), the three *m*CGPC samples showed similar capacities near 1 mmol/g. A slight increase in the CO_2 adsorption capacity was

https://doi.org/10.1021/acsomega.3c01083
ACS Omega 2023, 8, 21664−21676

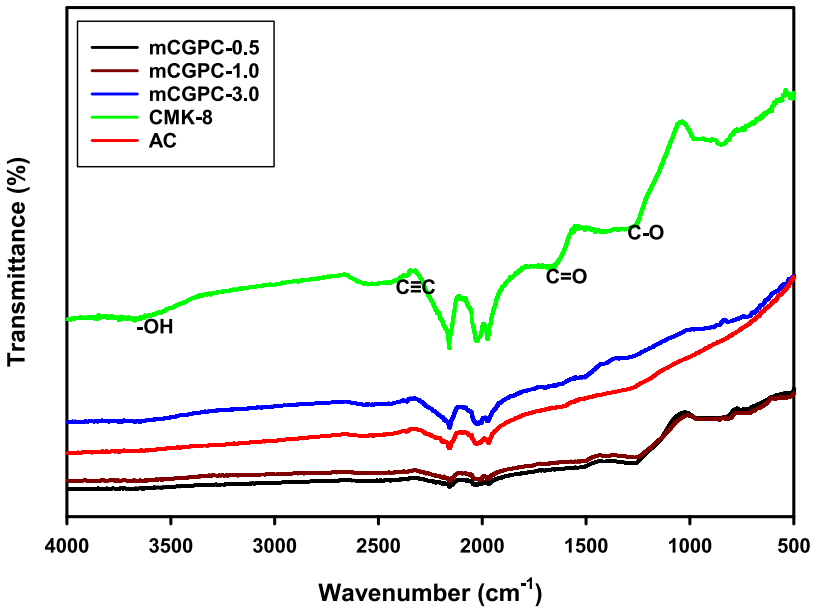

Figure 5. ATR/FTIR spectra of *m*CGPC, CMK-8, and AC materials.

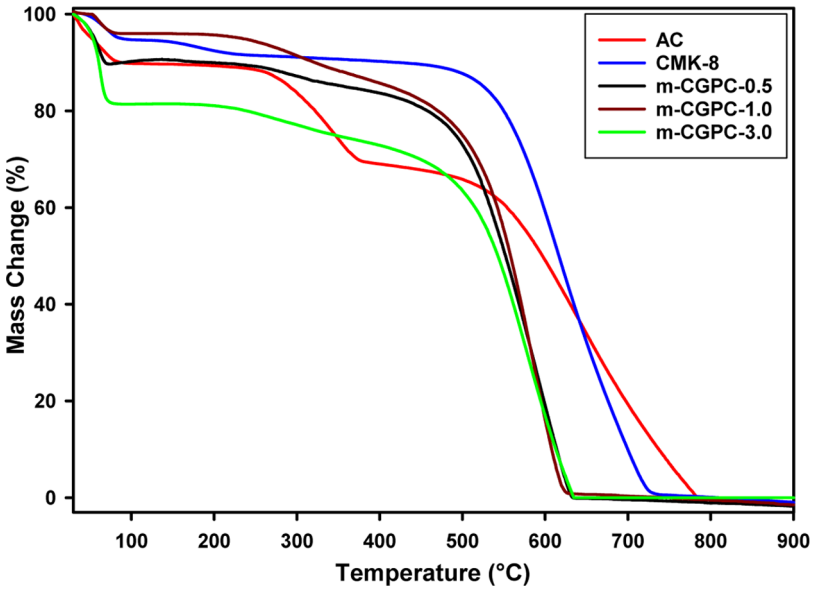

Figure 6. TGA profiles of *m*CGPC-*x*, CMK-8, and AC materials.

observed with increasing CG amount used for sample preparation, which is possibly a result of the increased surface area and pore volume. In general, the AC surface area and porosity are based on the carbon precursors, synthesis conditions, and the activation method. In this work, the AC used for comparison was synthesized from peat-based carbon (steam-activated). Many carbon manufacturers produce activated carbons from different sources based on the targeted applications. The CO_2 adsorption capacity and the thermal stability would vary due to the differences in surface and porosity properties.[55] For instance, the CO_2 adsorption capacity of biochar-derived AC is reported to be 0.61 mmol/g in.[56] The AC used in this work showed a low CO_2 adsorption capacity due to its lower surface area and low pore volume. The pore diameter was also very low, making CO_2 adsorption difficult. In general, AC is mostly microporous with a high micropore volume and possesses a lower adsorption capacity of CO_2 with a low surface area and pore diameter. The isotherms of *m*CGPCs had an almost similar pattern in Figure 9a,b for *m*CGPC-3.0, with the CO_2 uptake being slightly lower than the other two *m*CGPCs at the low pressures (up to 500 mbar), after which the uptake improves. This indicates that CO_2 interaction with *m*CGPC-3.0 is more active on the higher pressure side though the differences among the three *m*CGPCs are minimal.

The comparison of Figure 9a,b indicates that, when the temperature increases in the adsorption experiment, the CO_2 adsorption capacity is reduced. This is indicative of physisorption that is predominantly known to be exothermic in nature.

Figure 10 presents the nitrogen adsorption capacities of the materials, where the values are lower than those for CO_2 adsorption. The results are summarized in Table 4. CMK-8 had the highest adsorption capacity for N_2, while AC had the

https://doi.org/10.1021/acsomega.3c01083
ACS Omega 2023, 8, 21664−21676

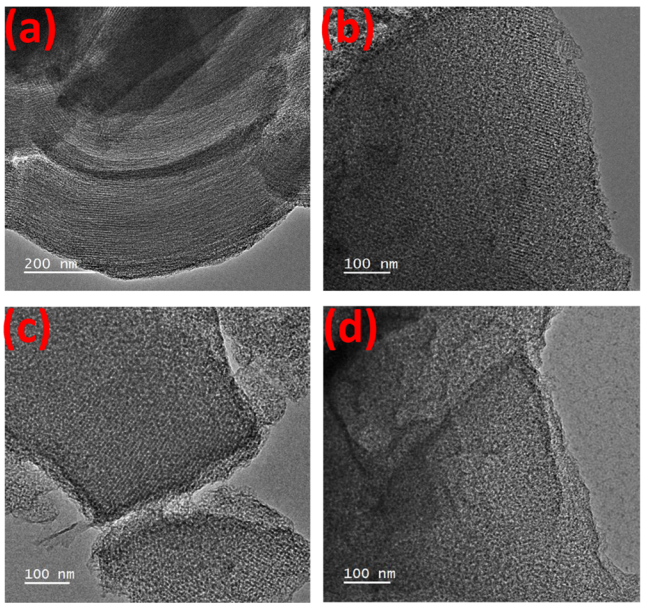

Figure 7. TEM images of (a) CMK-8, (b) *m*CGPC-0.5, (c) *m*CGPC-1.0, and (d) *m*CGPC-3.0.

lowest. The *m*CGPC-3.0 sample showed the lowest adsorption capacity for N_2 among the *m*CGPC materials. The low affinity of the adsorbents for N_2 means that the CO_2/N_2 selectivity will be high, as indicated in Table 4, which is a desired characteristic of an adsorbent for CO_2 capture from combustion exhaust gases. Among the mCGPC samples, Table 4 indicates that *m*CGPC-3.0 had the highest CO_2 adsorption capacity together with the highest CO_2/N_2 selectivity.

Table 3. Textural Properties of Adsorbents

sample	[a] S_{BET} (m^2/g)	[b] V_{total} (cm^3/g)	[c] V_{micro} (cm^3/g)	[d] average pore diameter (nm)
AC	515.7	0.262	0.112	2.04
CMK-8	1085.7	1.027	0.049	3.78
*m*CGPC-0.5	377.6	0.510	0.022	5.40
*m*CGPC-1.0	454.4	0.699	0.034	6.15
*m*CGPC-3.0	562.1	0.785	0.072	5.58

[a]BET surface area calculated over the pressure range 0.05−0.1 P/P_0. [b]Total pore volume at P/P_0 = 0.99. [c]Micropore volume. [d]Average pore size calculated from N_2 adsorption isotherms using the NLDFT method.

The pure component isosteric heat of adsorption was calculated using the Clausius−Clapeyron equation (eq 4), and its value for each adsorbent is shown in Figure 11.

$$\ln(P) = -\frac{\Delta H}{RT} + C \tag{4}$$

In this equation, ΔH corresponds to the enthalpy of adsorption in kJ/mol at a specific quantity of adsorbed CO_2; P and T are,

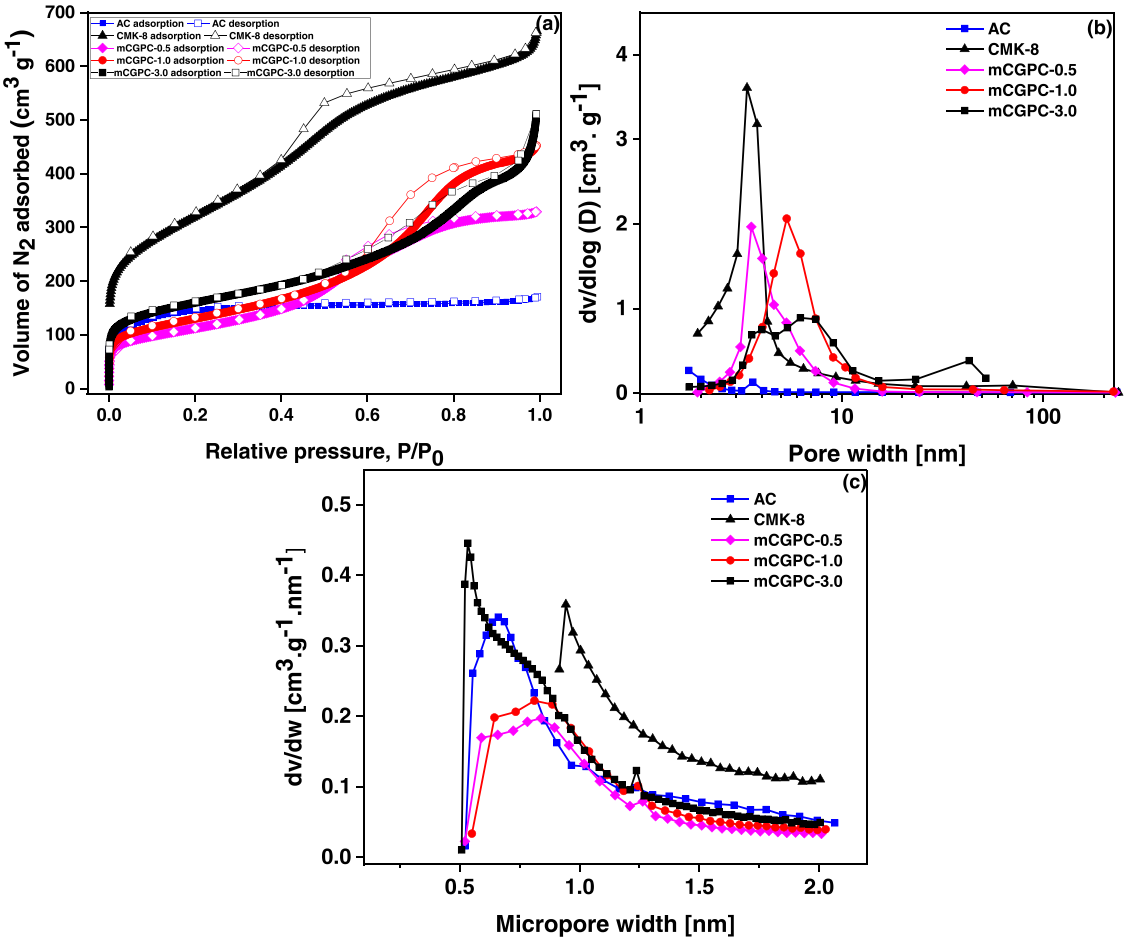

Figure 8. (a) N_2 adsorption−desorption at 77 K. (b) Mesopore size distribution. (c) Micropore size distribution.

https://doi.org/10.1021/acsomega.3c01083
ACS Omega 2023, 8, 21664−21676

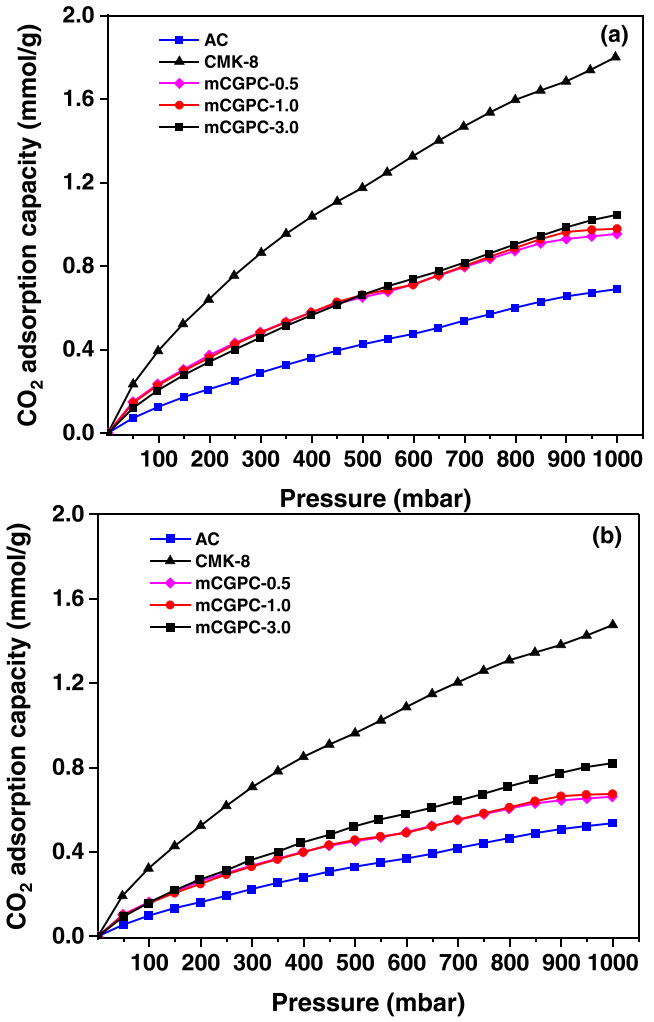

Figure 9. CO_2 adsorption capacity of adsorbents at (a) 25 °C and (b) 45 °C up to 1 bar.

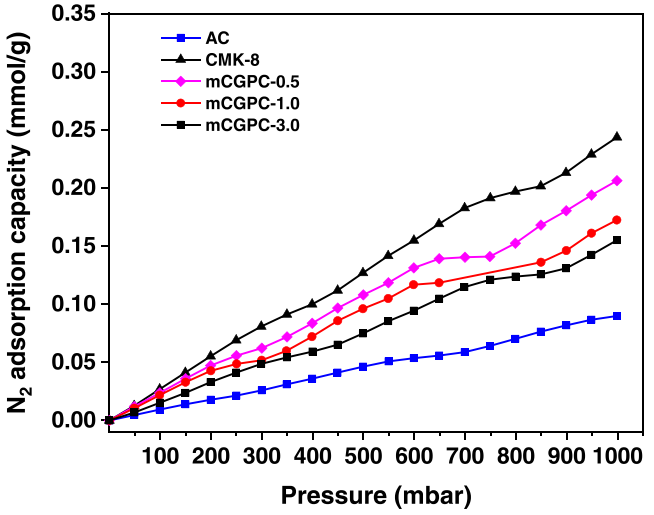

Figure 10. N_2 adsorption capacity of adsorbents at 25 °C and up to 1 bar in order to evaluate their CO_2/N_2 selectivity.

respectively, the absolute pressure in bar and temperature in K; R is the universal gas constant; and C is the integration constant. The isosteric heat of CO_2 adsorption was determined from the slope of $\ln(P)$ vs. $1/T$ curves at fixed amounts of

Table 4. CO_2 and N_2 Adsorption Capacities and CO_2/N_2 Selectivity at 1 bar and 25 °C

sample	CO_2 adsorption capacity at 1 bar (mmol/g)	N_2 adsorption capacity at 1 bar (mmol/g)	CO_2/N_2 selectivity at 1 bar
AC	0.689	0.090	7.66
CMK-8	1.800	0.244	7.38
*m*CGPC-0.5	0.954	0.206	4.63
*m*CGPC-1.0	0.978	0.172	5.69
*m*CGPC-3.0	1.045	0.155	6.74

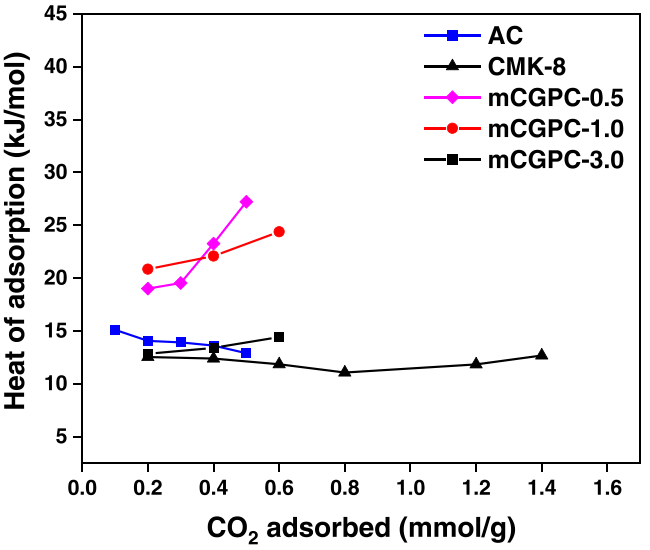

Figure 11. Heat of adsorption for different amounts of CO_2 adsorbed on the materials.

adsorbed CO_2 based on the adsorption isotherms at different temperatures. The heat of adsorption indicates the affinity of the adsorbent to the adsorbate. The adsorbent, AC, CMK-8, and *m*CGPC (3.0) had similar heats of adsorption in the range of 12−15 kJ/mol for different amounts of CO_2 on the adsorbents, while *m*CGPC-0.5 and *m*CGPC-1.0 had slightly higher heats of adsorption in the range of 19−27 kJ/mol. The relatively low heats of adsorption for all of the materials are indicative of the physisorption process, where the heat of adsorption remains generally between 10 and 40 kJ/mol. Additionally, the low heat of adsorption values confirm that these adsorbents are good candidates for pressure swing adsorption with less energy duties for their regeneration. Among the *m*CGPC samples, *m*CGPC-3.0 had the lowest heat of adsorption, which indicates that it would require less energy to regenerate and would thus be the preferred one among the *m*CGPC samples.

For an adsorbent, it is important to have a high regeneration efficiency so that it could be used over numerous adsorption−desorption cycles. All of the adsorbents were tested for five cycles of pressure swing adsorption (PSA), as shown in Figure 12. In this study, all of the adsorbents were found to retain the original CO_2 adsorption capacity even after the 5th cycle. Thus, CO_2 molecules desorb easily from the adsorbents without any surface accumulation during the regeneration process. All of these adsorbents were regenerated under high vacuum conditions without applying any activation temperature.

https://doi.org/10.1021/acsomega.3c01083
ACS Omega 2023, 8, 21664−21676

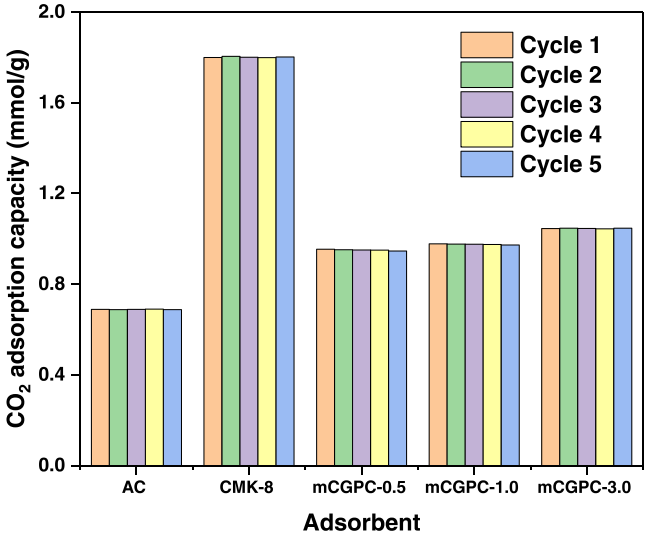

Figure 12. PSA regeneration cycles.

3.3. Modeling of the CO_2 Adsorption Isotherm. The Langmuir and Freundlich isotherm models were used to match the experimental data in order to determine a suitable adsorption isotherm model for CO_2 adsorption on the AC-, CMK-8-, and *m*CGPC-based adsorbents. One of the simplest models, the Langmuir model (eq 5), assumes monolayer adsorption on a homogeneous surface and that all active sites are identical for adsorbate molecules to bind to, giving them an equal adsorption energy. In the Freundlich model (eq 6), a heterogeneous surface is assumed, and adsorption takes place at locations with various adsorption energies.

$$q_e = \frac{q_m k_L P_{CO_2}}{1 + k_L P_{CO_2}} \quad (5)$$

$$q_e = k_F P_{CO_2}^{1/n} \quad (6)$$

where q_e is the equilibrium adsorption capacity in mmol/g, q_m is the monolayer adsorption capacity in mmol/g, P_{CO_2} is the CO_2 partial pressure in mbar, k_L is the Langmuir adsorption constant in $mbar^{-1}$ or affinity constant related to the energy of adsorption, K_F is the Freundlich adsorption constant in mmol g^{-1} $mbar^{-1/n}$, and n is the heterogeneity factor and can be used to evaluate the adsorption favorability of the adsorbents. Indicatively, n = 2−8 denotes strong affinity, n = 1 denotes moderate affinity, and n < 1 denotes poor affinity. Figure 13 shows the experimental CO_2 adsorption isotherm data of the AC-, CMK-8-, and *m*CGPC-based adsorbents at 25 °C and up to 1 bar fitted with Langmuir and Freundlich models. The model parameters and R^2 values are presented in Table 5.

Both the Langmuir[57] and Freundlich models suit the experimental data from Figure 13 and Table 5 well. By examining the R^2 values, it can be determined that the Freundlich model, which has R^2 values close to 1, is the one that best fits the data from the CO_2 adsorption isotherm. Additionally, the considerable surface heterogeneity in the adsorbents, which is confirmed by the n values in the range of 1.5, shows that CO_2 may be adsorbed with moderate heat of adsorption values in the range of 12−15 kJ/mol as explored in the heat of adsorption section. The analogous results obtained in our previous work[58] on ordered hierarchical nanostructured silica (OHNS) had an n value of 2.55 and heat of adsorption less than 16 kJ/mol.

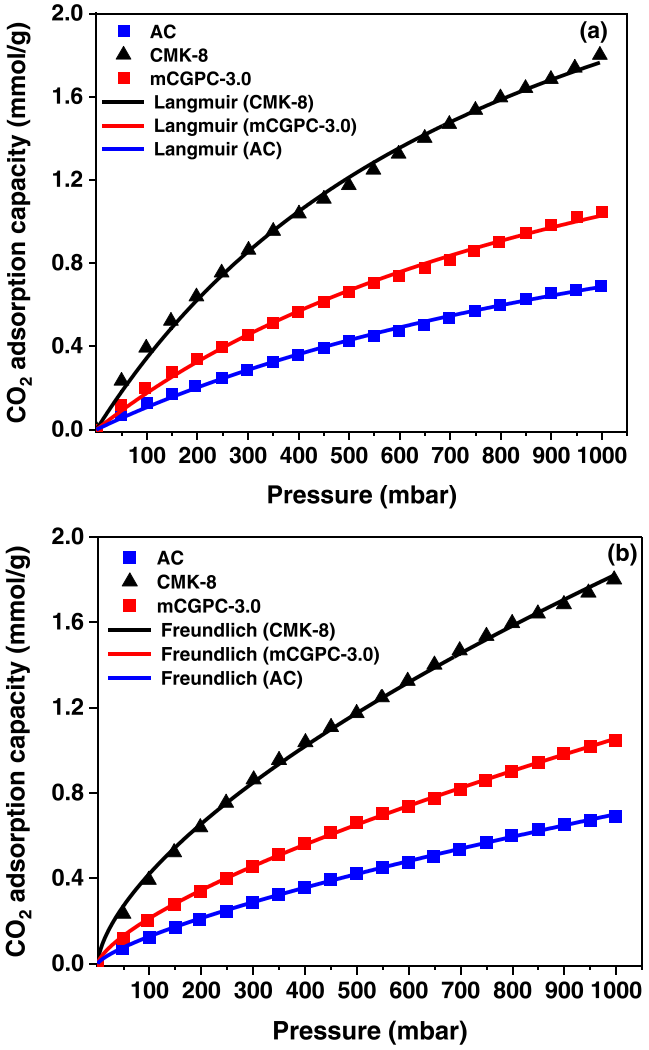

Figure 13. Experimental CO_2 adsorption data at 25 °C up to 1 bar and (a) Langmuir and (b) Freundlich models.

Table 5. Langmuir and Freundlich Model Parameters of AC-, CMK-8-, and *m*CGPC-Based Adsorbents at 25 °C

	Langmuir model parameters			Freundlich model parameters		
sample	q_m	k_L	R^2	K_F	n	R^2
AC	1.71	0.00067	0.998	0.00432	1.36	0.999
CMK-8	3.26	0.00119	0.997	0.02263	1.57	0.999
*m*CGPC-3.0	2.23	0.00086	0.997	0.00872	1.44	0.999

4. CONCLUSIONS

Crude bioglycerol is a waste from biodiesel production and a very useful and cheap alternative for carbon production from an environmental aspect. In summary, we have successfully synthesized ordered mesoporous carbons (*m*CGPCs) using crude glycerol as a carbon precursor via the hard template method. The physicochemical properties of the materials were thoroughly characterized by various analytical techniques. The XRD and RAMAN results depicted the carbon structure and nature of the porous materials, where the materials were found to have a partially graphitic and partially amorphous character.

https://doi.org/10.1021/acsomega.3c01083
ACS Omega 2023, 8, 21664−21676

The TEM images demonstrated a well-ordered porous structure for both *m*CGPCs and the reference material, CMK-8. The N_2 sorption isotherms confirmed the mesoporous nature and high porosity of the carbon materials. Finally, we evaluated the CO_2 adsorption performance of all of the synthesized materials and found that *m*CGPC-3.0 exhibited superior physical adsorption capacity compared to other *m*CGPCs and activated carbons, making it a promising candidate for CO_2 capture applications. Overall, the results suggest that *m*CGPCs synthesized from crude glycerol are viable alternatives to traditional carbon precursors for the synthesis of mesoporous carbons with excellent properties for CO_2 capture. The high CO_2/N_2 selectivity of this material also indicates its suitability for selective CO_2 capture and storage from combustion exhaust gases.

AUTHOR INFORMATION

Corresponding Authors

Prabhu Azhagapillai − *Department of Chemistry, Khalifa University of Science & Technology, Abu Dhabi 127788, U.A.E.;* orcid.org/0000-0002-6210-8821; Email: azhagapillai.prabhu@ku.ac.ae

Abhijeet Raj − *Department of Chemical Engineering, Khalifa University of Science & Technology, Abu Dhabi 127788, U.A.E.; Department of Chemical Engineering, Indian Institute of Technology Delhi, New Delhi 110016, India; Center for Catalysis and Separation, Khalifa University of Science & Technology, Abu Dhabi 127788, U.A.E.;* orcid.org/0000-0002-1470-0513; Email: raj@iitd.ac.in

Mirella Elkadi − *Department of Chemistry, Khalifa University of Science & Technology, Abu Dhabi 127788, U.A.E.;* Email: mirella.elkadi@ku.ac.ae

Authors

K. Suresh Kumar Reddy − *Department of Chemical Engineering, Khalifa University of Science & Technology, Abu Dhabi 127788, U.A.E.; Center for Catalysis and Separation, Khalifa University of Science & Technology, Abu Dhabi 127788, U.A.E.;* orcid.org/0000-0003-0956-6521

Gerardo D. J. Guerrero Pena − *Department of Chemistry, Khalifa University of Science & Technology, Abu Dhabi 127788, U.A.E.*

Rukayat S. Bojesomo − *Department of Chemistry, Khalifa University of Science & Technology, Abu Dhabi 127788, U.A.E.;* orcid.org/0000-0002-9649-170X

Dalaver H. Anjum − *Center for Catalysis and Separation and Department of Physics, Khalifa University of Science & Technology, Abu Dhabi 127788, U.A.E.*

Georgios N. Karanikolos − *Department of Chemical Engineering, Khalifa University of Science & Technology, Abu Dhabi 127788, U.A.E.; Center for Catalysis and Separation, Khalifa University of Science & Technology, Abu Dhabi 127788, U.A.E.; Research and Innovation Center on CO2 and H2 (RICH), Khalifa University, Abu Dhabi 127788, U.A.E.; Department of Chemical Engineering, University of Patras, Patras 26500, Greece;* orcid.org/0000-0001-5823-7076

Mohamed I. Ali − *Department of Mechanical Engineering, Khalifa University of Science & Technology, Abu Dhabi 127788, U.A.E.*

Complete contact information is available at: https://pubs.acs.org/10.1021/acsomega.3c01083

Notes

The authors declare no competing financial interest.

ACKNOWLEDGMENTS

The authors acknowledge the financial support by Khalifa University, UAE, through the Award #CIRA-2020-106 project led by Dr. M.E.

REFERENCES

(1) Welsby, D.; Price, J.; Pye, S.; Ekins, P. Unextractable fossil fuels in a 1.5 °C world. *Nature* **2021**, *597*, 230−234.

(2) Walsh, B.; Ciais, P.; Janssens, I. A.; Peñuelas, J.; Riahi, K.; Rydzak, F.; van Vuuren, D. P.; Obersteiner, M. Pathways for balancing CO2 emissions and sinks. *Nat. Commun.* **2017**, *8*, No. 14856.

(3) Du, J.; Haley, B. A.; Mix, A. C.; Walczak, M. H.; Praetorius, S. K. Flushing of the deep Pacific Ocean and the deglacial rise of atmospheric CO2 concentrations. *Nat. Geosci.* **2018**, *11*, 749−755.

(4) Webley, P. A. Adsorption technology for CO2 separation and capture: a perspective. *Adsorption* **2014**, *20*, 225−231.

(5) Bakhtyari, A.; Mofarahi, M.; Lee, C.-H. CO2 Adsorption by Conventional and Nanosized Zeolites. In *Advances in Carbon Capture*; Rahimpour, M. R.; Farsi, M.; Makarem, M. A., Eds.; Woodhead Publishing, 2020; Chapter 9, pp 193−228.

(6) Lee, S.-Y.; Park, S.-J. A review on solid adsorbents for carbon dioxide capture. *J. Ind. Eng. Chem.* **2015**, *23*, 1−11.

(7) Boot-Handford, M. E.; Abanades, J. C.; Anthony, E. J.; Blunt, M. J.; Brandani, S.; Mac Dowell, N.; Fernández, J. R.; Ferrari, M.-C.; Gross, R.; Hallett, J. P.; Haszeldine, R. S.; Heptonstall, P.; Lyngfelt, A.; Makuch, Z.; Mangano, E.; Porter, R. T. J.; Pourkashanian, M.; Rochelle, G. T.; Shah, N.; Yao, J. G.; Fennell, P. S. Carbon capture and storage update. *Energy Environ. Sci.* **2014**, *7*, 130−189.

(8) Gęca, M.; Wiśniewska, M.; Nowicki, P. Biochars and activated carbons as adsorbents of inorganic and organic compounds from multicomponent systems—A review. *Adv. Colloid Interface Sci.* **2022**, *305*, No. 102687.

(9) Ferro-García, M. A.; Rivera-Utrilla, J.; Bautista-Toledo, I.; Moreno-Castilla, C. Adsorption of humic substances on activated carbon from aqueous solutions and their effect on the removal of Cr (III) ions. *Langmuir* **1998**, *14*, 1880−1886.

(10) Gibson, J. A. A.; Mangano, E.; Shiko, E.; Greenaway, A. G.; Gromov, A. V.; Lozinska, M. M.; Friedrich, D.; Campbell, E. E. B.; Wright, P. A.; Brandani, S. Adsorption Materials and Processes for Carbon Capture from Gas-Fired Power Plants: AMPGas. *Ind. Eng. Chem. Res.* **2016**, *55*, 3840−3851.

(11) Samanta, A.; Zhao, A.; Shimizu, G. K. H.; Sarkar, P.; Gupta, R. Post-Combustion CO2 Capture Using Solid Sorbents: A Review. *Ind. Eng. Chem. Res.* **2012**, *51*, 1438−1463.

(12) Moon, S.-H.; Shim, J.-W. A novel process for CO2/CH4 gas separation on activated carbon fibers—electric swing adsorption. *J. Colloid Interface Sci.* **2006**, *298*, 523−528.

(13) Chang, B.; Shi, W.; Yin, H.; Zhang, S.; Yang, B. Poplar catkin-derived self-templated synthesis of N-doped hierarchical porous carbon microtubes for effective CO2 capture. *Chem. Eng. J.* **2019**, *358*, 1507−1518.

(14) Xu, Y.; Yang, Z.; Zhang, G.; Zhao, P. Excellent CO2 adsorption performance of nitrogen-doped waste biocarbon prepared with different activators. *J. Cleaner Prod.* **2020**, *264*, No. 121645.

(15) Petrovic, B.; Gorbounov, M.; Masoudi Soltani, S. Impact of Surface Functional Groups and Their Introduction Methods on the Mechanisms of CO2 Adsorption on Porous Carbonaceous Adsorbents. *Carbon Capture Sci. Technol.* **2022**, *3*, No. 100045.

(16) Sani, S.; Liu, X.; Li, M.; Stevens, L.; Sun, C. Synthesis and characterization of three-dimensional interconnected large-pore mesoporous cellular lignin carbon materials and their potential for CO2 capture. *Microporous Mesoporous Mater.* **2023**, *347*, No. 112334.

(17) Wang, X.; Zeng, W.; Kong, X.; Xin, C.; Dong, Y.; Hu, X.; Guo, Q. Development of Low-Cost Porous Carbons through Alkali

Activation of Crop Waste for CO2 Capture. *ACS Omega* **2022**, *7*, 46992−47001.
(18) Hack, J.; Maeda, N.; Meier, D. M. Review on CO2 Capture Using Amine-Functionalized Materials. *ACS Omega* **2022**, *7*, 39520−39530.
(19) Liu, L.; Deng, Q.-F.; Ma, T.-Y.; Lin, X.-Z.; Hou, X.-X.; Liu, Y.-P.; Yuan, Z.-Y. Ordered mesoporous carbons: citric acid-catalyzed synthesis, nitrogen doping and CO2 capture. *J. Mater. Chem.* **2011**, *21*, 16001−16009.
(20) Gang, D.; Uddin Ahmad, Z.; Lian, Q.; Yao, L.; Zappi, M. E. A review of adsorptive remediation of environmental pollutants from aqueous phase by ordered mesoporous carbon. *Chem. Eng. J.* **2021**, *403*, No. 126286.
(21) Ma, T.-Y.; Liu, L.; Yuan, Z.-Y. Direct synthesis of ordered mesoporous carbons. *Chem. Soc. Rev.* **2013**, *42*, 3977−4003.
(22) Wan, Y.; Shi, Y.; Zhao, D. Supramolecular Aggregates as Templates: Ordered Mesoporous Polymers and Carbons. *Chem. Mater.* **2008**, *20*, 932−945.
(23) Ryoo, R.; Joo, S. H.; Jun, S. Synthesis of Highly Ordered Carbon Molecular Sieves via Template-Mediated Structural Transformation. *J. Phys. Chem. B* **1999**, *103*, 7743−7746.
(24) Ryoo, R.; Hoon Joo, S. Nanostructured Carbon Materials Synthesized from Mesoporous Silica Crystals by Replication. In *Studies in Surface Science and Catalysis*; Terasaki, O., Ed.; Elsevier, 2004; Vol. *148*, pp 241−260.
(25) Lezanska, M.; Wloch, J.; Szymański, G.; Szpakowska, I.; Kornatowski, J. Properties of CMK-8 carbon replicas obtained from KIT-6 and pyrrole at various contents of ferric catalyst. *Catal. Today* **2010**, *150*, 77−83.
(26) Li, H.; Sakamoto, Y.; Li, Y.; Terasaki, O.; Thommes, M.; Che, S. Synthesis of carbon replicas of SBA-1 and SBA-7 mesoporous silicas. *Microporous Mesoporous Mater.* **2006**, *95*, 193−199.
(27) Kaneda, M.; Tsubakiyama, T.; Carlsson, A.; Sakamoto, Y.; Ohsuna, T.; Terasaki, O.; Joo, S. H.; Ryoo, R. Structural Study of Mesoporous MCM-48 and Carbon Networks Synthesized in the Spaces of MCM-48 by Electron Crystallography. *J. Phys. Chem. B* **2002**, *106*, 1256−1266.
(28) Zhou, L.; Li, H.; Yu, C.; Zhou, X.; Tang, J.; Meng, Y.; Xia, Y.; Zhao, D. Easy synthesis and supercapacities of highly ordered mesoporous polyacenes/carbons. *Carbon* **2006**, *44*, 1601−1604.
(29) Warren, S. C.; Messina, L. C.; Slaughter, L. S.; Kamperman, M.; Zhou, Q.; Gruner, S. M.; DiSalvo, F. J.; Wiesner, U. Ordered Mesoporous Materials from Metal Nanoparticle−Block Copolymer Self-Assembly. *Science* **2008**, *320*, 1748−1752.
(30) Choma, J.; Górka, J.; Jaroniec, M. Mesoporous carbons synthesized by soft-templating method: Determination of pore size distribution from argon and nitrogen adsorption isotherms. *Microporous Mesoporous Mater.* **2008**, *112*, 573−579.
(31) Fuertes, A. B. Synthesis of ordered nanoporous carbons of tunable mesopore size by templating SBA-15 silica materials. *Microporous Mesoporous Mater.* **2004**, *67*, 273−281.
(32) Janus, R.; Natkański, P.; Wądrzyk, M.; Lewandowski, M.; Łątka, P.; Kuśtrowski, P. Effect of solvent polarity in formation of perfectly ordered CMK-3 and CMK-5 carbon replicas by precipitation polycondensation of furfuryl alcohol. *Microporous Mesoporous Mater.* **2022**, *329*, No. 111542.
(33) Li, F.; van der Laak, N.; Ting, S.-W.; Chan, K.-Y. Varying carbon structures templated from KIT-6 for optimum electrochemical capacitance. *Electrochim. Acta* **2010**, *55*, 2817−2823.
(34) Schmidt, W.; Amenitsch, H. High Dynamics of Vapor Adsorption in Ordered Mesoporous Carbon CMK-5: A Small Angle X-ray Scattering Study. *J. Phys. Chem. C* **2020**, *124*, 21418−21425.
(35) Wu, R.; Ye, Q.; Wu, K.; Dai, H. Potassium-modified ordered mesoporous carbon materials (K-CMK-3): Highly efficient adsorbents for NO adsorption at low temperatures. *J. Solid State Chem.* **2021**, *294*, No. 121844.
(36) Dahiya, S.; Kumar, A. N.; Shanthi Sravan, J.; Chatterjee, S.; Sarkar, O.; Mohan, S. V. Food waste biorefinery: Sustainable strategy for circular bioeconomy. *Bioresour. Technol.* **2018**, *248*, 2−12.
(37) Xiong, X.; Yu, I. K. M.; Tsang, D. C. W.; Bolan, N. S.; Sik Ok, Y.; Igalavithana, A. D.; Kirkham, M. B.; Kim, K.-H.; Vikrant, K. Value-added chemicals from food supply chain wastes: State-of-the-art review and future prospects. *Chem. Eng. J.* **2019**, *375*, No. 121983.
(38) Mansir, N.; Teo, S. H.; Rashid, U.; Saiman, M. I.; Tan, Y. P.; Alsultan, G. A.; Taufiq-Yap, Y. H. Modified waste egg shell derived bifunctional catalyst for biodiesel production from high FFA waste cooking oil. A review. *Renewable Sustainable Energy Rev.* **2018**, *82*, 3645−3655.
(39) Gonçalves, M.; Castro, C. S.; Boas, I. K. V.; Soler, F. C.; Pinto, E. D. C.; Lavall, R. L.; Carvalho, W. A. Glycerin waste as sustainable precursor for activated carbon production: Adsorption properties and application in supercapacitors. *J. Environ. Chem. Eng.* **2019**, *7*, No. 103059.
(40) Chen, J.; Yan, S.; Zhang, X.; Tyagi, R. D.; Surampalli, R. Y.; Valéro, J. R. Chemical and biological conversion of crude glycerol derived from waste cooking oil to biodiesel. *Waste Manage.* **2018**, *71*, 164−175.
(41) Ignat, M.; Van Oers, C. J.; Vernimmen, J.; Mertens, M.; Potgieter-Vermaak, S.; Meynen, V.; Popovici, E.; Cool, P. Textural property tuning of ordered mesoporous carbon obtained by glycerol conversion using SBA-15 silica as template. *Carbon* **2010**, *48*, 1609−1618.
(42) Lee, D.-W.; Jin, M.-H.; Park, J. C.; Lee, C.-B.; Oh, D.; Lee, S.-W.; Park, J.-W.; Park, J.-S. Waste-Glycerol-Directed Synthesis of Mesoporous Silica and Carbon with Superior Performance in Room-Temperature Hydrogen Production from Formic Acid. *Sci. Rep.* **2015**, *5*, No. 15931.
(43) Jermy, B. R.; Cho, D.-R.; Bineesh, K. V.; Kim, S.-Y.; Park, D.-W. Direct synthesis of vanadium incorporated three-dimensional KIT-6: A systematic study in the oxidation of cyclohexane. *Microporous Mesoporous Mater.* **2008**, *115*, 281−292.
(44) Kumaresan, L.; Prabhu, A.; Palanichamy, M.; Murugesan, V. Mesoporous Ti-KIT-6 molecular sieves: Their catalytic activity in the epoxidation of cyclohexene. *J. Taiwan Inst. Chem. Eng.* **2010**, *41*, 670−675.
(45) Li, C.; Rath, P. C.; Lu, S.-X.; Patra, J.; Su, C.-Y.; Bresser, D.; Passerini, S.; Chang, J.-K. Ordered nano-structured mesoporous CMK-8 and other carbonaceous positive electrodes for rechargeable aluminum batteries. *Chem. Eng. J.* **2021**, *417*, No. 129131.
(46) Rath, P. C.; Mishra, M.; Saikia, D.; Chang, J. K.; Perng, T.-P.; Kao, H.-M. Facile fabrication of titania-ordered cubic mesoporous carbon composite: effect of Ni doping on photocatalytic hydrogen generation. *Int. J. Hydrogen Energy* **2019**, *44*, 19255−19266.
(47) Azhagapillai, P.; Al Shoaibi, A.; Chandrasekar, S. Surface functionalization methodologies on activated carbons and their benzene adsorption. *Carbon Lett.* **2021**, *31*, 419−426.
(48) Konggidinata, M. I.; Chao, B.; Lian, Q.; Subramaniam, R.; Zappi, M.; Gang, D. D. Equilibrium, kinetic and thermodynamic studies for adsorption of BTEX onto Ordered Mesoporous Carbon (OMC). *J. Hazard. Mater.* **2017**, *336*, 249−259.
(49) Koyuncu, D. D. E.; Okur, M. Removal of AV 90 dye using ordered mesoporous carbon materials prepared via nanocasting of KIT-6: Adsorption isotherms, kinetics and thermodynamic analysis. *Sep. Purif. Technol.* **2021**, *257*, No. 117657.
(50) Almeida, R. K. S.; Melo, J. C. P.; Airoldi, C. A new approach for mesoporous carbon organofunctionalization with maleic anhydride. *Microporous Mesoporous Mater.* **2013**, *165*, 168−176.
(51) Saikia, D.; Wang, T.-H.; Chou, C.-J.; Fang, J.; Tsai, L.-D.; Kao, H.-M. A comparative study of ordered mesoporous carbons with different pore structures as anode materials for lithium-ion batteries. *RSC Adv.* **2015**, *5*, 42922−42930.
(52) Phan, T. N.; Gong, M. K.; Thangavel, R.; Lee, Y. S.; Ko, C. H. Enhanced electrochemical performance for EDLC using ordered mesoporous carbons (CMK-3 and CMK-8): Role of mesopores and mesopore structures. *J. Alloys Compd.* **2019**, *780*, 90−97.
(53) Thommes, M.; Kaneko, K.; Neimark, A. V.; Olivier, J. P.; Rodriguez-Reinoso, F.; Rouquerol, J.; Sing, K. S. W. Physisorption of gases, with special reference to the evaluation of surface area and pore

https://doi.org/10.1021/acsomega.3c01083
ACS Omega 2023, 8, 21664−21676

size distribution (IUPAC Technical Report). *Pure Appl. Chem.* **2015**, *87*, 1051−1069.
(54) Ren, Z.; Jia, B.; Zhang, G.; Fu, X.; Wang, Z.; Wang, P.; Lv, L. Study on adsorption of ammonia nitrogen by iron-loaded activated carbon from low temperature wastewater. *Chemosphere* **2021**, *262*, No. 127895.
(55) Sahoo, S. Experimental investigation on different activated carbons as adsorbents for CO2 capture. *Therm. Sci. Eng. Prog.* **2022**, *33*, No. 101339.
(56) Shahkarami, S.; Azargohar, R.; Dalai, A. K.; Soltan, J. Breakthrough CO2 adsorption in bio-based activated carbons. *J. Environ. Sci.* **2015**, *34*, 68−76.
(57) Langmuir, I. The adsorption of gases on plane surfaces of glass, mica and platinum. *J. Am. Chem. Soc.* **1918**, *40*, 1361−1403.
(58) Reddy, K. S. K.; Varghese, A. M.; Ogungbenro, A. E.; Karanikolos, G. N. Aminosilane-Modified Ordered Hierarchical Nanostructured Silica for Highly-Selective Carbon Dioxide Capture at Low Pressure. *ACS Appl. Eng. Mater.* **2023**, *1*, 720−733.

https://doi.org/10.1021/acsomega.3c01083
ACS Omega 2023, 8, 21664−21676